Highly pixelated, untethered tactile interfaces for an on-skin telehaptic system

Hanbit Jin
Electronics and Telecommunications Research Institute https://orcid.org/0000-0003-1445-3804
Yunjeong Kim
Electronics and Telecommunications Research Institute
Wooseup Youm
Electronics and Telecommunications Research Institute https://orcid.org/0000-0002-4891-6566
Yulim Min
University of Science and Technology (UST)
Chaehyun Lim
Electronics and Telecommunications Research Institute(ETRI)
Chan-Hwa Hong
Electronics and Telecommunications Research Institute(ETRI)
Seyoung Kwon
Korea Advanced Institute of Science and Technology(KAIST)
Gyeongseok Park
Korea Advanced Institute of Science and Technology(KAIST)
Steve Park
Korea Advanced Institute of Science and Technology https://orcid.org/0000-0002-1428-592X
Hye Jin Kim (nolawara@etri.re.kr)
Electronics and Telecommunications Research Institute

Article

Keywords: skin-conformable tactile sensor, actuator array, untethered tactile communication

Posted Date: October 19th, 2021

DOI: https://doi.org/10.21203/rs.3.rs-952562/v1

Abstract

For highly immersive telehaptic applications, skin-integrated, untethered, and highly pixelated transducer devices that can record and generate tactile stimuli are required. Here, we propose a skin-conformable tactile sensor and actuator array with high spatial resolution of 1.8 mm for realising untethered tactile communication on human skin. The tactile sensors are designed to exhibit ultra-flexibility and bimodal sensitivity to static and dynamic pressure. The actuators are miniaturised to sub-millimetre scale to provide sophisticated, high spatiotemporal resolution tactile feedback over a centimetre square area of the fingertip with the capacity to generate vibrotactile feedback under an external load of up to 529 kPa. Short time Fourier transform analysis showed that our telehaptic system can transmit various types of tactile stimuli, such as the shape of objects and letters, textures of fabrics, and vibration patterns with high fidelity.

Introduction

Interest in virtual interaction has grown rapidly in various fields, including education, healthcare, retail, robotics, and manufacturing[1–9]. Performing tasks in a virtual environment can provide indirect but realistic experiences in a low-cost, contactless, and convenient manner[10,11]. Conventional virtual/augmented reality (VR/AR) systems rely mainly on visual and auditory stimuli. The degree of immersion and accuracy in virtual interactions can be significantly enhanced by providing tactile feedback[12–15]. However, the tactile feedback system is at a preliminary stage compared to audio and video technologies. Further improvements in functionalities, such as high-resolution, multimodal feedback, and real-time communication, are required to enable sophisticated tangible interactions in a distant place and/or virtual place. We refer to a tactile feedback system with these features as a telehaptic system.

The ultimate goal of the telehaptic system is to transmit sophisticated and near-realistic tactile sensations from one user to another. The key ability of a telehaptic transducer relies on precisely monitoring the spatiotemporal physical deformations occurring at the soft skin surface and reproducing them in remote places. To impart the capability to sense and actuate tactile information on and to the skin without disrupting natural hand functionality, mechanically flexible, lightweight, and untethered designs are required. Although telehaptic transducer devices based on rigid sensors and actuators, such as desktop haptic devices[16,17], tablet-type surface haptic devices[17–19], and wearable gloves[21–23] have already been demonstrated, they still suffer from the constraints of user motion originating from rigid and tethered designs.

To address the mechanical compliance and untethering issue of haptic transducers, tremendous efforts have been made to develop materials and novel structural designs for skin-attachable haptic interfaces. For instance, soft materials have been introduced to achieve mechanical flexibility, such as electroactive polymer (EAP)-based actuators[24–28], shape memory polymers (SMP)[29], and pneumatic/hydraulic

actuators based on microfluidic channels[29–31]. However, these soft actuators suffer from common operational issues, such as high operating voltage and large size of air compression equipment.

Improving the spatial resolution of a pixelated actuator array is another major challenge in terms of achieving immersive tactile feedback. Miniaturised coil and magnet-based 32 actuators have been embedded in silicone elastomer and wirelessly operated and powered by near-field communication (NFC), enabling untethered and skin conformable designs[3]. However, the pixel size of these devices is of the order of centimetres, which is too large for application onto narrow and sensitive areas such as the hand and fingertips. Electrostatic and pneumatic type high-resolution actuators have also been reported. Flexible hydraulically amplified electrostatic actuators have achieved a 6 mm pitch resolution to fit at least one actuator on a fingertip[31]. A 4 × 4 pneumatic tactile display with Braille standard resolution (2.5 mm) using a bistable electroactive polymer (BSEP) thin film has also been reported[33]. However, these devices are limited in their operating speed, originating from the slow hydraulic, pneumatic flow and thermal change.

Piezoelectric actuators are an alternative method to generate high spatiotemporal tactile patterns with low operational burden. High-performance piezoceramic-based actuators have been studied to provide fast response and dynamic movements with accelerations as high as 500 m/s^2 and slew rates in the microsecond range at micrometre displacement. This is due to the very fast piezoelectric ionic shift in and the high stiffness of the materials.[34] Wide frequency range up to several 10 kHz, and capability of miniaturisation are also advantageous for generating high-resolution and crisp haptic response necessary for emulated buttons and textures.[35] However, a major drawback of piezoceramic actuators for on-skin applications is their planar and rigid format. To overcome these limitations, ultrathin $Pb[Zr_xTi_{1-x}]O_3$ (PZT) membranes have been utilised as mechanical sensors and actuators with high spatial resolution[36]. However, the thin membrane of PZT leads to insufficient output force for haptic applications, although it was effective for modulus sensing in medical applications. Hence, transmitting tactile stimuli using high-resolution on-skin piezoelectric actuators still remains a key challenge in terms of achieving both mechanical compliance and sufficient performance.

Here, we demonstrate a skin-attachable, untethered telehaptic system that consists of an ultra-flexible bimodal tactile sensor and a flexible tactile actuator array that can acquire and regenerate tactile stimuli patterns with 1.8 mm pitch and 1.55 ms high spatiotemporal resolution. The actuator array is designed to be wirelessly coupled with an ultra-flexible bimodal sensor array that consists of a fast adaptive (FA) and slow adaptive (SA) mechanoreceptor-like pressure sensor array that can simultaneously monitor static and dynamic pressures with high spatial resolution. The actuator array can generate sinusoidal vibration patterns as well as near-realistic high-resolution tactile stimuli patterns corresponding to the signals acquired from each sensor pixel. The sensor-actuator interworking system is mechanically flexible, lightweight, and wirelessly operated for immersive telehaptics. Finally, the developed system enables real-time transmission of high-definition tactile stimuli. Various types of spatiotemporal tactile patterns, including textures of fabrics, and pressing, clicking, and flapping of butterfly wings generated by a load

cell and a commercial haptic device (PowerHap^{TM}, TDK Corp.), were acquired using the high-resolution bimodal sensor array. They were then regenerated by the actuator array with high fidelity, as proven by short-time Fourier transform spectral analysis.

Results And Discussion

Design and fabrication of skin-attachable tactile sensor and actuator array

The telehaptic system is designed to transmit tactile stimuli in real time using a wirelessly coupled on-skin tactile sensor and actuator, as shown in Fig. 1. The basic principle of the on-skin telehaptic interface is shown in Fig. 1a. The skin-attached bimodal sensor array detects friction-induced vibrations, impacts, and normal pressure generated during contact between the fingertip and an object. The acquired tactile signals were amplified and transmitted to the actuator array using Bluetooth communication. The actuator array generates vibration patterns for rendering the delivered tactile information composed of various frequencies, amplitudes, and spatial distributions. The sensor array is designed to have selective sensitivity to static and dynamic pressure for recording complex tactile signals by mimicking human mechanoreceptors, Merkel's discs and Pacinian corpuscles. For the static pressure sensor, chemically grafted Polypyrrole (Ppy) on elastomeric micro-pyramids (made with PDMS, polydimethylsiloxane) was exploited because of its reproducibility and high sensitivity based on previous studies[37,38]. Unlike many other conductive materials, Ppy can chemically react with the hydroxyl groups on the PDMS surface; therefore, higher durability and repeatability are expected when using Ppy.[37] Using this material, a piezoresistive pressure sensor array is designed into miniaturised sensing pixels with individual pixel area of 1.045 mm^2.

To monitor the dynamic pressure, the piezoelectric polymer PVDF-TrFE was chosen because of its superior mechanical flexibility[39] and process compatibility (Supplementary Figure 1) for a high-resolution array. The annealing process was important for the crystallinity and piezoelectric characteristics of PVDF-TrFE thin film. A 3 μm PVDF-TrFE thin film was annealed in a vacuum oven at an optimized annealing temperature of 130 ℃ (Supplementary Figure 2). The sensor array contains static and dynamic pressure sensors arranged in a chessboard pattern densely packed into an area of a centimetre square to resolve and monitor the spatial distribution of fine tactile stimuli (Fig. 1b, c). Unlike the previously reported flexible multi-layered bimodal sensor arrays[40,41] that have relatively high thickness of 120 μm, our sensor pixels are integrated on a single layer of ultrathin polyimide substrate (~4 μm) to achieve a higher bending compliance, which is beneficial for making a conformal contact with the skin surface[42]. Owing to the ultra-flexibility of the sensor array, it can be conformally laminated on a curvilinear fingertip surface, as shown in Fig. 1d, which is beneficial for acquiring reliable tactile information without mechanical distortion at the interface between the skin and the object. The collected tactile information is amplified and wirelessly transmitted by the signal processing module located at the back of the hand, realising the untethered operation of the telehaptic system (Fig. 1e).

In the high-resolution tactile actuator array, the actuating pixels are fabricated using miniaturized piezoelectric ceramics with a sub-millimetre length scale (0.98 mm), and these actuators are assembled into a 32 channel-array on a flexible polyimide substrate. Because piezoelectric actuators are processed into 32 layers using standard piezo-ceramic manufacturing techniques, the actuators are rigid. However, since they are mounted on a flexible substrate via a surface mounting process (i.e. using anisotropic conductive film (ACF) bonding process (Supplementary Figure 3)), a flexible and skin-conformable actuator array can be fabricated. Thereafter, actuator array can be embedded into elastomer by pouring PDMS on top, which acts as a protection layer and as vibration isolator. Owing to its high piezoelectric coefficient (47525 pC/N in average) and small pixel size (< 1 mm^2), piezo-ceramic actuators can generate spatially distributed tactile stimuli patterns with high resolution (1.8 mm pitch) over a wide dynamic frequency range (1 Hz–1 kHz) (Fig. 1f, g). The tactile actuator array is designed to have mechanical flexibility to directly adhere onto a fingertip and deliver spatially segmented actuation on the curved surface (Fig. 1h). The acquired tactile signals from the sensor array are wirelessly transmitted to the actuator array's drive module located on the back of the hand (Fig. 1i) that supplies up to 40 V_{pp} for each actuator pixel.

Detection of static/dynamic pressure for acquiring tactile stimuli

The ultra-flexible bimodal (UFB) tactile sensor array can detect static and dynamic pressures simultaneously and selectively. Fig. 2a, b show the working mechanisms of the piezoresistive static pressure sensor and the piezoelectric dynamic pressure sensor, respectively. For the piezoresistive pressure sensor, the Ppy-coated micropyramids are placed on top of the interdigitated electrodes. When pressure is applied to the sensor, the tip of the pyramid is deformed from a triangular shape to that of a trapezoid, and no significant cracking was observed on the surface of Ppy even under 40 kPa of pressure, as shown in Supplementary Figure 1c. The contact area between the electrode and the conductive pyramid increases as the pressure increases, resulting in a decrease in the contact resistance (R_c) (Fig. 2a). As applied pressure increases from 3 kPa to 80 kPa, the contact resistance was observed to continuously decrease from 1 MΩ to 100 kΩ. The highest value of sensitivity is 13.93 kPa^{-1} in the low-pressure range of 3–10 kPa, and the sensitivity decreases to 4.65 kPa^{-1} (10–30 kPa) and 0.32 kPa^{-1} (30–80 kPa) in the high-pressure range, as shown in Fig. 2c. Over the entire sensing range of 3–80 kPa (which is the recognisable pressure range of human touch[43]), our sensor is capable of differentiating a pressure change of <1 kPa.

For the piezoelectric dynamic pressure sensors, the PVDF-TrFE film was patterned and the mechanism of electric charge generation by the piezoelectric effect was exploited. The sensor provides a fast response and a wide range of frequency detection when dynamic vibration is applied. It is shown that the rising time of the patterned dynamic pressure sensor is 250 μs as shown in Fig. 2d. The human tactile response time is 385 μs [44], which implies that the sensor has a sufficiently fast response and is capable of precisely capturing tactile stimuli. The fast response is important because unwanted effects similar to

motion sickness may occur if the time interval between the visual and tactile feedback exceeds 1 ms[43]. Furthermore, vibration can be detected with a sufficient average SNR of 15.4 dB (=10logS/N) in the frequency range from 1 Hz to 1 kHz, as shown in Fig. 2e and Supplementary Figure 4. The decrease in the output current in the high frequency range is attributed to the inherent frequency dependence of the vibrator that is applied to the bimodal sensor, showing a reduced force with increasing frequency.

To evaluate the simultaneous sensing of static and dynamic pressure, a static pressure change and a 200 Hz vibration were applied to the neighbouring static and dynamic sensor pixels by repeatedly pressing the vibrator mounted on the sensor as shown in Fig. 2f. Static pressure changes were measured in terms of the voltage across the reference resistor in a voltage divider circuit as shown by the red and orange lines in Figs. 2g, h. The vibrations detected by the dynamic sensor pixel is indicated by the green line in Figs. 2g, h. Since the centre of the vibrator is closer to the static-L, the amplitude of static-L is larger than that of static-R. There is a limitation in detection of static pressure and vibration simultaneously with a unimodal sensor. For instance, static pressure can be estimated from the signal envelop of dynamic sensor. But it is hard to precisely detect the absolute magnitude of the static pressure as the amplitude of dynamic sensor can be distorted by the influence of the triboelectric effect and capacitance coupling. Therefore, a bimodal sensor capable of both static and dynamic pressure sensing is required to detect a wide range of complex tactile stimuli.

The mechanical compliance of the ultra-flexible and ultra-thin bimodal sensor enables conformable attachment onto the soft skin surface, as shown in Fig. 2i. The ultra-thin sensor is also advantageous for enabling natural deformation of skin upon application of small area pressure (i.e. thick sensors have higher stiffness preventing natural deformation of skin). To verify the mechanical compliance of the ultra-flexible bimodal sensor, the compressive strain-stress curve of a flexible and ultra-flexible substrate laminated on a silicone elastomer was measured. The flexible substrate is a 125 μm thick PI film used for industrial standard FPCB, and the ultra-flexible substrate is 4 μm-thick PI film. The strain-stress characteristics of the silicone elastomer (Eco-flex 00-30, modulus: 210 kPa (measured) and 100 kPa (reference)[45]), which has a Young's modulus similar to that of human skin (epidermis modulus: 140 to 600 kPa[46]), was measured for reference, and each sample loaded on the elastomer was pressed by a load cell, as shown in Fig. 2j. The stresses of the flexible sensor, ultra-flexible sensor, and silicone elastomer were respectively 44, 24 and 21 kPa at 10% strain, as shown in the compressive strain-stress curve of Fig. 2k. This result confirms that the ultra-flexible sensor would only marginally affect the modulus of skin-like soft elastomers.

Sub-millimetre scale, high-resolution actuator array for generating vibrotactile stimuli

A single sub-mm actuator has a size of 0.980.980.8 mm (widthlengthheight) and average weight of 6.7 mg. It is a multi-layered piezoceramic actuator in which actuation displacement and output force is proportional to the piezoelectric coefficient and number of stacked ceramic layers (Fig. 3c

and Supplementary Figure 5). As shown in Fig. 3a and b, our actuator can stimulate an area of less than 1 mm^2 on the fingertip. The actuators are placed on the contact pad of a 125 μm-thick flexible and 4 μm-thick ultra-flexible substrate, and the electrical and mechanical connections are made by the reflow soldering and ACF transfer process, respectively, in a 1.8 mm pitch chessboard array (Supplementary Figure 6). Because the actuator pixels are embedded with PDMS, the vibration generated in each pixel can be isolated so that it is hardly transmitted to adjacent pixels (Supplementary Figure 7).

The characteristics of the actuator pixels were evaluated under mass and force loading in the operating voltage and frequency range of 5–60 V_{pp} and 100–1000 Hz, respectively. For practical applications, tactile actuators must endure external loads applied by human finger interactions. Our results confirm that our ceramic-based piezoelectric actuator is robust under an external load or contact force, which is a challenging issue for other soft or flexible actuators[47].

Fig. 3d shows the acceleration of a single actuator under vibration, driven at various peak-to-peak voltages (V_{pp}) at 200 Hz, when loaded with mass from 0.12 g to 0.92 g (see inset for schematic depiction). Above 10 V_{pp}, the accelerations are larger than the absolute limen (0.1 m/s^2 at 200 Hz), which is the threshold acceleration that humans can feel[49,50]. At 40 and 60 V_{pp}, the acceleration of the actuator with 0.92 g mass loading was 1.19 m/s^2 and 2.04 m/s^2, respectively, which is 10 times and 20 times higher than the absolute limen. The maximum input voltage was limited to 60 V_{pp} because larger voltages can cause degradation of the actuator performance.

Fig. 3e shows the displacement of a single actuator under force loading from 0 kPa to 592 kPa. Force was loaded on the top of the actuator with an anvil (contact area is 1 mm^2) as shown in the inset schematic of Fig. 3e. Interestingly, the acceleration and displacement were found to increase with the mass and force loading. This phenomenon can be well described by an influence of applied preload on piezoelectric stack actuator, where strain output is enhanced with an increase in mechanical preload and the maximum strain values can be obtained at an optimum preload[48]. Above 10 V_{pp}, the displacement is larger than the Pacinian threshold (150 nm at 200 Hz)[51,52] which is the displacement threshold. At 40 and 60 V_{pp} operation, the displacement of the actuator under 592 kPa of pressure was 755 nm and 1315 nm, respectively. Since the output displacement characteristics of the actuator was saturated at pressures larger than 592 kPa, external pressures were applied up to 592 kPa which means that it is the optimum preload for the actuator stack and a higher preload starts to impede the overall piezoelectric effect.[48] The sub-mm actuator showed a displacement larger than 970 nm in the frequency range from 100 Hz to 1 kHz. The displacement was found to slightly decrease as the operation frequency increased, as seen in Fig. 3f. The displacement at 1 kHz decreased by 4% from the displacement at 100 Hz, which implies the actuator system can cover up to 1 kHz without significant performance degradation.

Generating sufficient displacement to exceed the threshold for sensation at frequencies below 10 Hz is important to accurately deliver the static pressure tactile information. However, in this frequency range, since the mechanoreceptors require a large displacement of at least 40 μm for recognition[52], this is

unrealistic for piezoelectric actuators to achieve. To address this fundamental challenge, we introduce amplitude modulation in the form of envelops as depicted in Fig. 3g. Here, carrier frequency of 300 Hz and envelope frequency ranging from 1 Hz to 10 Hz was applied to the actuator since human can easily recognize 300 Hz vibration with threshold displacement of 150 nm, while our actuator can generate much larger displacement of up to 1.3 μm. Fig. 3h shows the FFT (fast Fourier transform) result of modulated signals for imparting the sensation of static pressure. Along with the carrier frequency peak (300 Hz), low frequency peaks at 1, 2, 3, 5, 7, and 10 Hz, are clearly visible in the FFT result.

Wireless tactile acquisition and rendering system for telehaptic communication

For realising immersive telehaptic communication, proper designing of signal processing units and wireless connections are crucial for transmitting the complex tactile stimuli with high similarity and low delay. In the proposed telehaptic system, the tactile sensor and actuator were wirelessly coupled by signal processing modules, as shown in Fig. 4. The module for processing and transmitting the sensor signals is composed of a pre-amplifier, microcontroller, and Bluetooth low-energy (BLE), as shown in Fig. 4a, b. Pre-amplifiers for bimodal pressure sensor array have been designed as two different circuits for each sensing type. The static pressure was measured by a voltage divider and a voltage follower circuit to cover wide range of sensor output impedance, as shown in Supplementary Figure 8b. The dynamic pressure was measured by using a high gain voltage-mode piezoelectric amplifier which can amplify pA-order charge generation, as shown in Supplementary Figure 8c. The module for the tactile actuator array is composed of an actuator driver, a microcontroller, and a BLE for generating vibrations in accordance with the transmitted sensor signals. The actuator driver distributed voltage inputs to each actuator pixel with maximum peak-to-peak voltage of 90 V. A LED driver is added to visualise the generated tactile patterns during telehaptic communication (Fig. 4c, d).

The telehaptic system has small delay time (< 1.55 ms), which is advantageous for preventing virtual reality sickness, and high similarity (> 80%) between detected and regenerated complex tactile stimuli, which implies the capability of accurate tactile communication. To measure the delay time of the wireless telehaptic system, a 50 Hz sine wave was applied to the dynamic sensor pixel using a vibrator, and the velocity of the vibration on the actuator was monitored using a 3D laser scanning vibrometer (LSV), during which the sensor signal was being wirelessly transmitted across a distance of 3 m, as shown in Fig. 4e. The delay time was 1.55 ms, which was measured by comparing the signal applied to the sensor with the signal regenerated by the actuator (Fig. 4f, g).

To verify the similarity of the acquired complex tactile signals and the regenerated tactile stimuli, a vibration signal pattern similar with a vibration of motorcycle was transmitted through the telehaptic system, as shown in the blue plot depicting the sensor signal (Fig. 4 (h)) and the red plot depicting the actuator's vibrational displacement (Fig. 4i). The correlation between the sensor signals and the actuator vibration signals (orange windows of Fig 4h, i, with the area name of S1, A1, S2 and A2) was calculated and shown in the correlation matrix correlogram from the Pearson correlation coefficient (PCC) (Fig. 4j). The correlation coefficients between S1-A1 and S2-A2 were both 0.8 and 0.81, and the correlation

coefficients of signal envelop for S1-A1 and S2-A2 were 0.97 and 0.91, respectively. In other words, when both amplitude and frequency considered, the wireless telehaptic system shows signal similarity of 80 % and 81 % between the acquired and generated tactile stimuli. On the other hand, when considering the amplitude only, our system show higher signal similarity of 97% and 91%. We have also tested the similarity of sine waves with various frequencies (100, 200, 300, 400, and 500 Hz) (Supplementary Figure 12). The correlation coefficient was 0.99, 0.96, 0.99, 0.92, and 0.82 at 100, 200, 300, 400, and 500 Hz, respectively. In other words, the signals reproduced by the actuator shows similarities of more than 90% to the sensor signals, except for 500 Hz. At 500 Hz, the actuator signals included a beat wave with a beat frequency of 7 Hz, which may have originated from the noise in the optical measurement system, i.e., the doppler signal and speckle noise of the laser vibrometer.[53]

Demonstration of a wireless telehaptic system

Fig. 5a shows a skin-attachable wireless telehaptic system demonstrating the transmission of spatial pressure distribution. Volunteer 1 (left) attaches the UFB tactile sensor on the fingertip of the index finger and rolls a plastic stick on it. The UFB tactile sensor acquires the spatial distribution of the static pressure changes and transmits the signals to the actuator processing module. The tactile information is reproduced by a tactile actuator attached on the fingertip of volunteer 2 (right) and visualised by an LED display placed on the back side of the hand of volunteer 2 (Supplementary movie 1). Fig. 5b shows a magnified image of the pressed position of the UFB sensor on the finger and the illuminated LED (inset of Fig. 5b). The UFB sensor can detect more complex shapes due to its highly pixelated static pressure sensor array, such as alphabet letters (I, V, U), as shown in Fig. 5c, and the actuator array can regenerate acquired tactile signals, as shown in the LSV scanning image (Fig. 5d, Supplementary video 4). The red colour in Fig. 5d indicates a larger vibrational amplitude.

The UFB tactile sensor can also detect dynamic vibrations that are relevant to texture and motion. The volunteer who attached the UFB tactile sensor rubbed the surface of three different fabrics (Fig. 5e, f, Supplementary movie 2, 3). To amplify the surface vibration, the PDMS grating pattern was laminated on the surface of the sensor (Supplementary Figure 9). The roughness of the fabric increases with fabric number; for example, fabric 3 is the roughest among the fabrics used in the study (Supplementary Figure 10). To further investigate the correlation between the sensor and actuator signals after transmitting the texture information of the fabrics to the actuator, short-term Fourier transform (STFT) analysis was conducted. Fig. 5g and 5h show the STFT results of the sensor signal and the actuator vibration. The main frequencies (f_{main}) of the sensor signals were 403, 326, and 229 Hz for fabrics 1, 2, and 3, respectively. The main frequency decreased when the sensor rubbed the rougher surface.[54] Similar to the sensor tendency, the main frequencies of the actuator signals were 400 Hz, 326 Hz, and 229 Hz (Supplementary Figure 11). The STFT patterns of the sensor and actuator signals show strong similarities, which indicates that the vibration feature has been successfully transmitted. Other complicated tactile stimuli such as press, click, and butterfly wing flap have been successfully

transmitted by the telehaptic system. Here, the pattern of press was generated by a pressure applying system with load cell, while tactile patterns of click and butterfly wing flap were generated by using sample waveforms of the vibration actuator (PowerHap^{TM}, TDK Corp, and BOS1901, Boreas technologies). The correlation coefficients of the envelop signals of the sensor and actuator were respectively 0.89, 0.98 and 0.93 for pressing, clicking and butterfly wing flapping patterns (Supplementary Figure 12, 13).

Conclusion

In this study, we demonstrated telehaptic communication with an on-skin platform. Ultra-flexible sensor array and miniaturised actuator array enable real-time tangible interactions with various tactile stimuli. The piezoresistive and piezoelectric hybridised pressure sensor array was used to detect the spatial distribution of static pressure levels and frequency information of vibrotactile stimuli at high resolution. A miniaturised 32-channel actuator array successfully regenerated the detected tactile stimuli signals. Although the miniaturized piezoelectric actuator can sufficiently generate high spatiotemporal vibration patterns above the detection limit of the skin, the displacement should be further improved for greater enhancement of tactile feelings, through designing displacement amplification mechanisms. The proposed sensor and actuator system can transmit and share tactile sensations remotely, which may open new avenues for tactile-based human-machine interface. The telehaptic platform can enable assisting the users with manual tasks, making people feel physically connected even over long distances, and enriching the feeling of presence in virtual environments like augmented/virtual reality (AR/VR).

Experimental Section

Fabrication of ultra-flexible bimodal (UFB) tactile sensor array

Ultra-flexible backplane

The polyimide precursor was spin-coated onto a carrier glass and cured to form a 2 μm-thick base layer. And Ti/Au (10 nm/200 nm) electrode and transmission line were fabricated on the base layer by photolithography, with an interdigitated (IDE) pattern with minimum line and space width of 50 and 100 μm, respectively. And 2 μm-thick PI was fabricated on the device for encapsulation layer and windows of contact electrode are opened by PI wet etching. After the fabrication of ultra-flexible backplane, it was peeled off from the carrier glass by laser lift off process with energy density of 180 mJ/cm^2 (KORONA^{TM} LLO, AP systems). The 32-channel sensor pixel array for static pressure sensor is arranged in 1.8 mm pitch and 4 additional pixels for dynamic pressure sensor are added between the pixels. The width and length of the IDE electrode pattern for the static pressure sensor are 0.25 and 1.1 mm, respectively. The gap between the two counter electrodes is 0.45 mm. The electrode size and gap were determined by considering pixel size, sensor sensitivity, and processability. Resistance change is proportional to area of the electrode pad, such that larger width and length are desirable for sensitivity, but the area is limited for high-resolution device fabrication. The gap was chosen to be 0.45 mm for sharing the backplane with

actuator array, which is the suitable size for the mounting process. For the dynamic pressure sensor, the gap between the counter electrode was set at 0.1 mm. The electrode pattern for the piezoelectric sensor has a narrower gap than that of the piezoresistive sensor because smaller gap is advantageous for detecting changes in electric field originated from piezoelectric material under pressure.

Static pressure sensor

A microstructured PDMS film was fabricated using a replica moulding process, i.e., soft photolithographic moulding. A Si wafer was etched using potassium hydroxide (KOH) solution to form micro-pyramid structures with a side wall angle of 54.7°. The PDMS pyramid soft mould was prepared by mechanically mixing the PDMS (Sylgard 184, Dow Corning) base solution and the curing agent (10:1 wt.%). It was cured at 80 °C for 3 h and lifted off the replica. The width and the gap of the micropyramid structure are both 100 μm. The pyramid sheet was prepared by spin-coating on a soft replica at 800 rpm for 30 s and heating in a convection oven at 80 °C. Polypyrrole (Pyrrole (98%), Sigma Aldrich) was coated on the cured 100-μm-thick micro pyramid film by depositing pyrrole monomer silane (Tridecafluoro-1,1,2,2,-tetrahydrooctyl trichlorosilane, Sigma Aldrich). The pyrrole was then polymerised in a pyrrole and oxidant solution (iron (III) chloride hexahydrate, Sigma Aldrich) at 25 °C.

Dynamic pressure sensor

The PVDF-TrFE solutions (20 wt.%) were prepared by dissolving 2 g of PVDF-TrFE copolymer pellets (75:25 (mol%), Piezotech) in 2-butanone (MEK, 99 +%, Sigma Aldrich) and acetone (1:1 (wt.%)). The PVDF-TrFE solution was spin-coated at 4000 rpm for 40 s and onto the IDE metal electrode substrate. The solution was sequentially degassed overnight under vacuum to eliminate the bubbles. The PVDF-TrFE films were crystalline, followed by annealing at 130 ℃ for 3h. After preparation of the PVDF-TrFE film, a 2-nm/200-nm-thick Ti/Au film was deposited by E-beam evaporation (KVET-C500200, Korea Vacuum) under a DC field of 10 kV at 9×10^{-7} Torr as an etch stop mask for reactive ion etching (RIE). The PVDF-TrFE film was etched under 10 sccm O_2 and 20 sccm CF_4 gas environments for 30 min with 20 W RF power. It was polarised under a DC field of 50 kV/mm at 25 °C for 3 h. Finally, the micro-pattern for enhanced texture perception was prepared by the PDMS micromolding process with line width, height, and spacing, each equal to 1 mm.

Fabrication of ultra-flexible sub-mm piezoelectric (UFP) tactile actuator array

Flexible Sub-mm piezoelectric tactile actuator Array

The sub-mm tactile actuator is a piezoelectric ceramic multilayer which is composed of 32 layers of lead zirconate titanate (PZT) ceramic with a thickness of 50 μm. Fabrication process of sub-mm tactile actuator is industrially standardized process of piezoelectric ceramic actuator. Firstly, green sheet of PZT slurry with top Ag electrode is laminated into 32-layer-stack and sintered in high temperature (~1200 ˚C). After the sintering process, the piezoelectric ceramic multilayer is cut into a die of dimensions 0.98 mm 0.98 mm 0.8 mm. Finally, contact electrodes (Ag) were sputtered on both sides of the ceramic block for connecting inner electrodes and on bottom for contact pad (designed by our group and manufactured by WiSOL Co., Ltd). The tactile actuator pixel was bonded together for double stack actuator and electrically connected by silver epoxy. Then, 32 actuator pixels are firmly anchored above the flexible printed circuit board (FPCB) by reflow soldering process for flexible actuator array. For the ultra-flexible actuator array, actuators are mounted on 3 μm-thick PI substrate with carrier glass by using adhesive conductive film (ACF) transfer process and peeled off from the carrier glass by using above mentioned laser lift off process (LLO).

Measurement of UFB tactile sensor array

Electrical characteristics

The static sensitivities of the bimodal pressure sensor were measured by a load cell pressure measurement station, which has a power supply (E3631A, Keysight) with a bias voltage of 2 V, a low-noise current preamplifier (SR570, Stanford Research Systems), and a force gauge (PI V-275.431, force range of 0.01 N to 10 N and resolution of 0.001 N (0.01 gf)).

The characteristics of the dynamic pressure sensors were acquired using a low-noise current preamplifier (SR570, Stanford Research Systems) and oscilloscope (DPO5054, Tektronics). We used a function generator (33220A, Agilent) and a piezo amplifier (E663, PI) to apply the dynamic frequency.

Mechanical characteristics

The strain-stress measurement setup consisted of a load cell pressure station with a force gauge and the signals were captured using a data acquisition system (DAQ).

Measurement of UFP tactile actuator array

Laser Scanning Vibrometer

The characteristics of the FST actuator array were investigated using a laser scanning vibrometer (LSV) system (PSV-400, PolyTech GmbH, Germany) with a laser scanning head (PSV-400), a scanning vibrometer controller (OFV-5000), and a junction box (PSV-400).

Wireless tactile acquisition and rendering system

The tactile sensor and actuator array were operated by a wireless tactile acquisition circuit board (Transmit Data, TX) and a tactile rendering circuit board (Receive Data, RX), respectively. The tactile TX circuit comprises of a pre-amplifier circuit, a microcontroller with Bluetooth communication system, a power management circuit to provide constant voltage, and a battery.

Signal processing and pre-amplifier circuit

The sensor signal acquired by the bimodal tactile sensor was amplified using a pre-amplifier circuit. A voltage mode amplifier (AD8643, Analog Devices) circuit was used for the dynamic pressure sensor, and a voltage divider and follower circuit were used for the static pressure sensor.

Microcontrollers and Bluetooth communication system

A microcontroller (nRF528321, Nordic semi) was mounted on a PCB board for data sampling (12-bit built-in ADC). The sampled data was transmitted to the RX board using a 2.4 GHz RF built-in Bluetooth module. The actuator driver (BOS1901, Boreas Technologies) for driving piezoelectric actuators is controlled by elevating the voltage from 3.3 V to a maximum voltage of 95 V_{pp}. The LED driver and the LED matrix (PIM442, PIMRONI Ltd) were used for the visualisation of tactile feedback. The brightness of the LED was controlled based on the spatial distribution and pressure level data received from the static pressure sensor array.

Power supply and regulation

The TX board was powered by a Li-polymer battery (TW401215, 15124 mm^2, 40 mAh), and the power was regulated by a boost and inverting converter. The RX board is composed of a 300 mAh Li-polymer battery, and a buck converter is used for power regulation.

Demonstration of wireless telehaptic system

Spatial recognition

Haptic communication was demonstrated with an ultra-flexible static/dynamic pressure sensor, a customised 32-channel amplifier, and a multi-morph piezoelectric actuator. The bimodal pressure sensor was connected to an amplifier. The noise of the signal is filtered, and the gain of the signal is controlled. The tactile stimuli information (sensor output) was recorded simultaneously using an oscilloscope (DPO-5054, Tektronics). The recognised information was transmitted to the actuator. The vibration of the

actuator was monitored using the LSV system. The monitored vibration information included vibration displacement for each point within the scanning area.

Texture recognition

To quantitatively analyse the average roughness of the three fabrics, the average maximum height of the 1.6 mm profile was measured using a confocal microscope (DCM-8, Leica).

The signals from the UFS attached to the fingertip were acquired while rubbing the three different fabrics in the same direction and transmitted to the FST.

Data availability

The data that support the plots within this paper and other findings of this study are available from the corresponding author upon reasonable request.

References

1. Howe, R. D. & Cutkosky, M. R. Dynamic tactile sensing: perception of fine surface features with stress rate sensing. *IEEE Trans. Robot. Autom.* **9**, 140–151 (1993).
2. Biswas, S. & Visell, Y. Emerging Material Technologies for Haptics. *Adv. Mater. Technol.* **4**, 1–30 (2019).
3. Yu, X. *et al.* Skin-integrated wireless haptic interfaces for virtual and augmented reality. *Nature* **575**, 473–479 (2019).
4. Steinbach, E. *et al.* Haptic communications. *Proc. IEEE* **100**, 937–956 (2012).
5. Van Der Meijden, O. A. J. & Schijven, M. P. The value of haptic feedback in conventional and robot-assisted minimal invasive surgery and virtual reality training: A current review. *Surg. Endosc.* **23**, 1180–1190 (2009).
6. Gavish, N. *et al.* Evaluating virtual reality and augmented reality training for industrial maintenance and assembly tasks. *Interact. Learn. Environ.* **23**, 778–798 (2015).
7. Kavanagh, S., Kavanagh, S., Luxton-Reilly, A., Wuensche, B. & Plimmer, B. A systematic review of Virtual Reality in education. *Themes Sci. Technol. Educ.* **10**, 85–119 (2017).
8. Liu, B. & Tanaka, J. Virtual Marker Technique to Enhance User Interactions in a Marker-Based AR System. *Appl. Sci. 2021, Vol. 11, Page 4379* **11**, 4379 (2021).
9. Na, W., Dao, N., Kim, J., Ryu, E. & Cho, S. Simulation and measurement: Feasibility study of Tactile Internet applications for mmWave virtual reality. *ETRI J.* **42**, 163–174 (2020).
10. Aebersold, M., Rasmussen, J. & Mulrenin, T. Virtual Everest: Immersive Virtual Reality Can Improve the Simulation Experience. *Clin. Simul. Nurs.* **38**, 1–4 (2020).

11. Gavish, N. *et al.* Evaluating virtual reality and augmented reality training for industrial maintenance and assembly tasks. *Interact. Learn. Environ.* **23**, 778–798 (2015).
12. Scheibe, R., Moehring, M. & Froehlich, B. Tactile feedback at the finger tips for improved direct interaction in immersive environments. *IEEE Symp. 3D User Interfaces* 2007 *- Proceedings, 3DUI 2007* 123–130 (2007) doi:10.1109/3DUI.2007.340784.
13. King, C. H. *et al.* Tactile feedback induces reduced grasping force in robot-assisted surgery. *IEEE Trans. Haptics* **2**, 103–110 (2009).
14. Liu, G., Sun, X., Wang, D., Liu, Y. & Zhang, Y. Effect of Electrostatic Tactile Feedback on Accuracy and Efficiency of Pan Gestures on Touch Screens. *IEEE Trans. Haptics* **11**, 51–60 (2018).
15. de Jesus Oliveira, V. A., Nedel, L. & Maciel, A. Assessment of an articulatory interface for tactile intercommunication in immersive virtual environments. *Comput. Graph.* **76**, 18–28 (2018).
16. Jarillo-Silva, A., Domínguez-Ramírez, O. A., Parra-Vega, V. & Ordaz-Oliver, J. P. PHANToM OMNI haptic device: Kinematic and manipulability. *CERMA 2009 - Electron. Robot. Automot. Mech. Conf.* 193–198 (2009) doi:10.1109/CERMA.2009.55.
17. Howard, B. M. & Vance, J. M. Desktop haptic virtual assembly using physically based modelling. *Virtual Real.* **11**, 207–215 (2007).
18. Jang, S., Kim, L. H., Tanner, K., Ishii, H. & Follmer, S. Haptic Edge Display for Mobile Tactile Interaction. *Proc. 2016 CHI Conf. Hum. Factors Comput. Syst.* doi:10.1145/2858036.
19. Kim, J. R. & Shin, S. Touch3D. in *ACM SIGGRAPH 2017 Posters* 1–2 (ACM, 2017). doi:10.1145/3102163.3102196.
20. Besse, N. *et al.* Understanding Graphics on a Scalable Latching Assistive Haptic Display Using a Shape Memory Polymer Membrane. *IEEE Trans. Haptics* **11**, 30–38 (2018).
21. Prattichizzo, D., Chinello, F., Pacchierotti, C. & Malvezzi, M. Towards Wearability in Fingertip Haptics: A 3-DoF Wearable Device for Cutaneous Force Feedback. *IEEE Trans. Haptics* **6**, 506–516 (2013).
22. Ozioko, O., Karipoth, P., Hersh, M. & Dahiya, R. Wearable Assistive Tactile Communication Interface Based on Integrated Touch Sensors and Actuators. *IEEE Trans. Neural Syst. Rehabil. Eng.* **28**, 1344–1352 (2020).
23. Choi, I., Hawkes, E. W., Christensen, D. L., Ploch, C. J. & Follmer, S. Wolverine: A wearable haptic interface for grasping in virtual reality. in 2016 *IEEE/RSJ International Conference on Intelligent Robots and Systems (IROS)* 986–993 (IEEE, 2016). doi:10.1109/IROS.2016.7759169.
24. Kim, O., Kim, S. J. & Park, M. J. Low-voltage-driven soft actuators. *Chem. Commun.* **54**, 4895–4904 (2018).
25. Yun, S. *et al.* A Soft and Transparent Visuo-Haptic Interface Pursuing Wearable Devices. *IEEE Trans. Ind. Electron.* **67**, 717–724 (2020).
26. Youn, J.-H., Mun, H. & Kyung, K.-U. A Wearable Soft Tactile Actuator With High Output Force for Fingertip Interaction. *IEEE Access* **9**, 30206–30215 (2021).

27. Zhao, H. *et al.* A Wearable Soft Haptic Communicator Based on Dielectric Elastomer Actuators. *Soft Robot.* **7**, 451–461 (2020).
28. Ji, X. *et al.* Untethered Feel-Through Haptics Using 18-μm Thick Dielectric Elastomer Actuators. *Adv. Funct. Mater.* 2006639 (2020) doi:10.1002/adfm.202006639.
29. Besse, N., Rosset, S., Zarate, J. J. & Shea, H. Flexible Active Skin: Large Reconfigurable Arrays of Individually Addressed Shape Memory Polymer Actuators. *Adv. Mater. Technol.* **2**, 1700102 (2017).
30. Sonar, H. A., Gerratt, A. P., Lacour, S. P. & Paik, J. Closed-Loop Haptic Feedback Control Using a Self-Sensing Soft Pneumatic Actuator Skin. https://home.liebertpub.com/soro **7**, 22–29 (2020).
31. Leroy, E., Hinchet, R. & Shea, H. Multimode Hydraulically Amplified Electrostatic Actuators for Wearable Haptics. *Adv. Mater.* 2002564 (2020) doi:10.1002/adma.202002564.
32. Low, J. H. *et al.* Hybrid Tele-Manipulation System Using a Sensorized 3-D-Printed Soft Robotic Gripper and a Soft Fabric-Based Haptic Glove. *IEEE Robot. Autom. Lett.* **2**, 880–887 (2017).
33. Qiu, Y., Lu, Z. & Pei, Q. Refreshable Tactile Display Based on a Bistable Electroactive Polymer and a Stretchable Serpentine Joule Heating Electrode. *ACS Appl. Mater. Interfaces* **10**, 24807–24815 (2018).
34. Pertsch, P. Piezoelectric Actuator Applications - Status 2018. in *ACTUATOR 2018; 16th International Conference on New Actuators* 25–27 (VDE, 2018).
35. WANG, D. *et al.* Haptic display for virtual reality: progress and challenges. *Virtual Real. Intell. Hardw.* **1**, 136–162 (2019).
36. Dagdeviren, C. *et al.* Conformal piezoelectric systems for clinical and experimental characterization of soft tissue biomechanics. *Nat. Mater.* **14**, 728–736 (2015).
37. Yang, J. C. *et al.* Microstructured Porous Pyramid-Based Ultrahigh Sensitive Pressure Sensor Insensitive to Strain and Temperature. *ACS Appl. Mater. Interfaces* **11**, 19472–19480 (2019).
38. Oh, J. *et al.* Highly Uniform and Low Hysteresis Piezoresistive Pressure Sensors Based on Chemical Grafting of Polypyrrole on Elastomer Template with Uniform Pore Size. *Small* 1901744 (2019) doi:10.1002/smll.201901744.
39. Ha, M. *et al.* Skin-Inspired Hierarchical Polymer Architectures with Gradient Stiffness for Spacer-Free, Ultrathin, and Highly Sensitive Triboelectric Sensors. *ACS Nano* **12**, 3964–3974 (2018).
40. Chun, S. *et al.* An artificial neural tactile sensing system. *Nat. Electron.* **4**, 429–438 (2021).
41. Chun, S. *et al.* Self-Powered Pressure- and Vibration-Sensitive Tactile Sensors for Learning Technique-Based Neural Finger Skin. *Nano Lett.* **19**, 3305–3312 (2019).
42. Kim, D.-H. *et al.* Dissolvable films of silk fibroin for ultrathin conformal bio-integrated electronics. *Nat. Mater.* **9**, 511–517 (2010).
43. Van Den Berg, D. *et al.* Challenges in Haptic Communications Over the Tactile Internet. *IEEE Access* **5**, 23502–23518 (2017).
44. Chan, A. H. S. & Ng, A. W. Y. Finger response times to visual, auditory and tactile modality stimuli. 1449–1454 (2012).

45. Vaicekauskaite, J., Mazurek, P., Vudayagiri, S. & Skov, A. L. Mapping the mechanical and electrical properties of commercial silicone elastomer formulations for stretchable transducers. *J. Mater. Chem. C* **8**, 1273–1279 (2020).
46. Kim, D.-H. *et al.* Epidermal Electronics. *Science (80-.).* **333**, 838–843 (2011).
47. Pyo, D., Ryu, S., Kyung, K.-U., Yun, S. & Kwon, D.-S. High-pressure endurable flexible tactile actuator based on microstructured dielectric elastomer. *Appl. Phys. Lett.* **112**, 061902 (2018).
48. Mitrovic, M., Carman, G. P. & Straub, F. K. Electromechanical characterization of piezoelectric stack actuators. in (ed. Wereley, N. M.) 586–601 (1999). doi:10.1117/12.350689.
49. Morioka, M. & Griffin, M. J. Thresholds for the perception of hand-transmitted vibration: Dependence on contact area and contact location. *Somatosens. Mot. Res.* **22**, 281–297 (2005).
50. Ko, H.-U., Chan Kim, H., Kim, J. & Kim, S.-Y. Miniaturized 3 × 3 array film vibrotactile actuator made with cellulose acetate for virtual reality simulators. *Smart Mater. Struct.* **24**, 055018 (2015).
51. Gescheider, G. A., Bolanowski, S. J., Pope, J. V. & Verrillo, R. T. A four-channel analysis of the tactile sensitivity of the fingertip: frequency selectivity, spatial summation, and temporal summation. *Somatosens. Mot. Res.* **19**, 114–124 (2002).
52. Van Duong, Q., Nguyen, V. P., Luu, A. T. & Choi, S. T. Audio-Tactile Skinny Buttons for Touch User Interfaces. *Sci. Rep.* **9**, 13290 (2019).
53. Rothberg, S. Numerical simulation of speckle noise in laser vibrometry. *Appl. Opt.* **45**, 4523 (2006).
54. Stoimenov, B. L., Maruyama, S., Adachi, K. & Kato, K. The roughness effect on the frequency of frictional sound. *Tribol. Int.* **40**, 659–664 (2007).

Figures

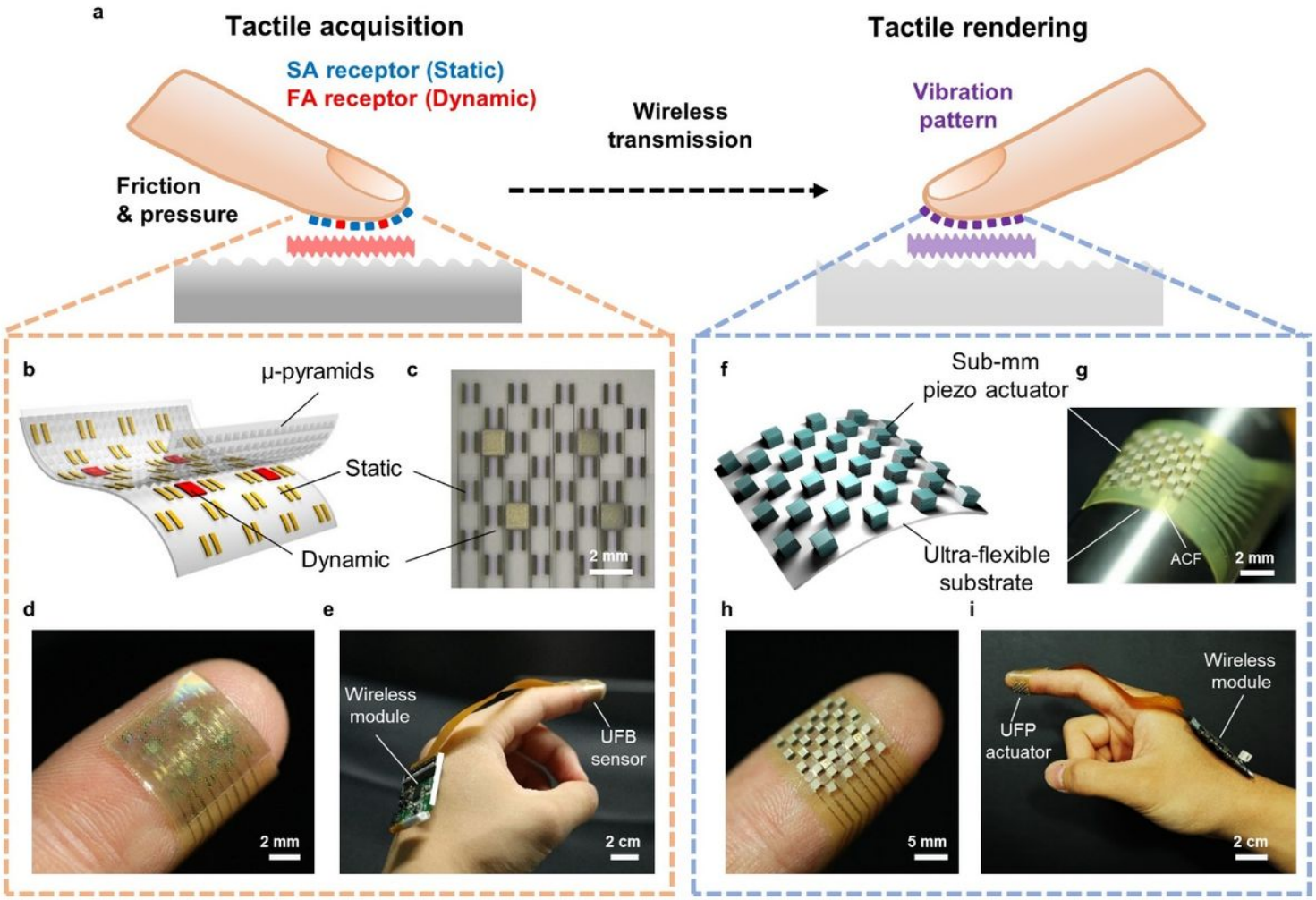

Figure 1

Ultra-flexible bimodal (UFB) tactile sensor and sub-mm tactile actuator array for telehaptic system. a, Schematic of telehaptic system composed of tactile acquisition (left) and rendering (right). b, 3D schematic of ultra-flexible bimodal (UFB) tactile sensor array. c, Optical microscopy image of the UFB tactile sensor array. d, Image of the UFB tactile sensor laminated on the fingertip. e, UFB tactile sensor with a wireless system attached to the hand for tactile acquisition. f, 3D schematic of ultra-flexible sub-mm piezoelectric (UFP) tactile actuator array. g, Image of the actuator array assembled on an ultra-flexible substrate. h, the ultra-flexible sub-mm tactile actuator array laminated on the fingertip. i, Sub-mm piezoelectric tactile actuator array with a wireless system attached to the hand for tactile rendering.

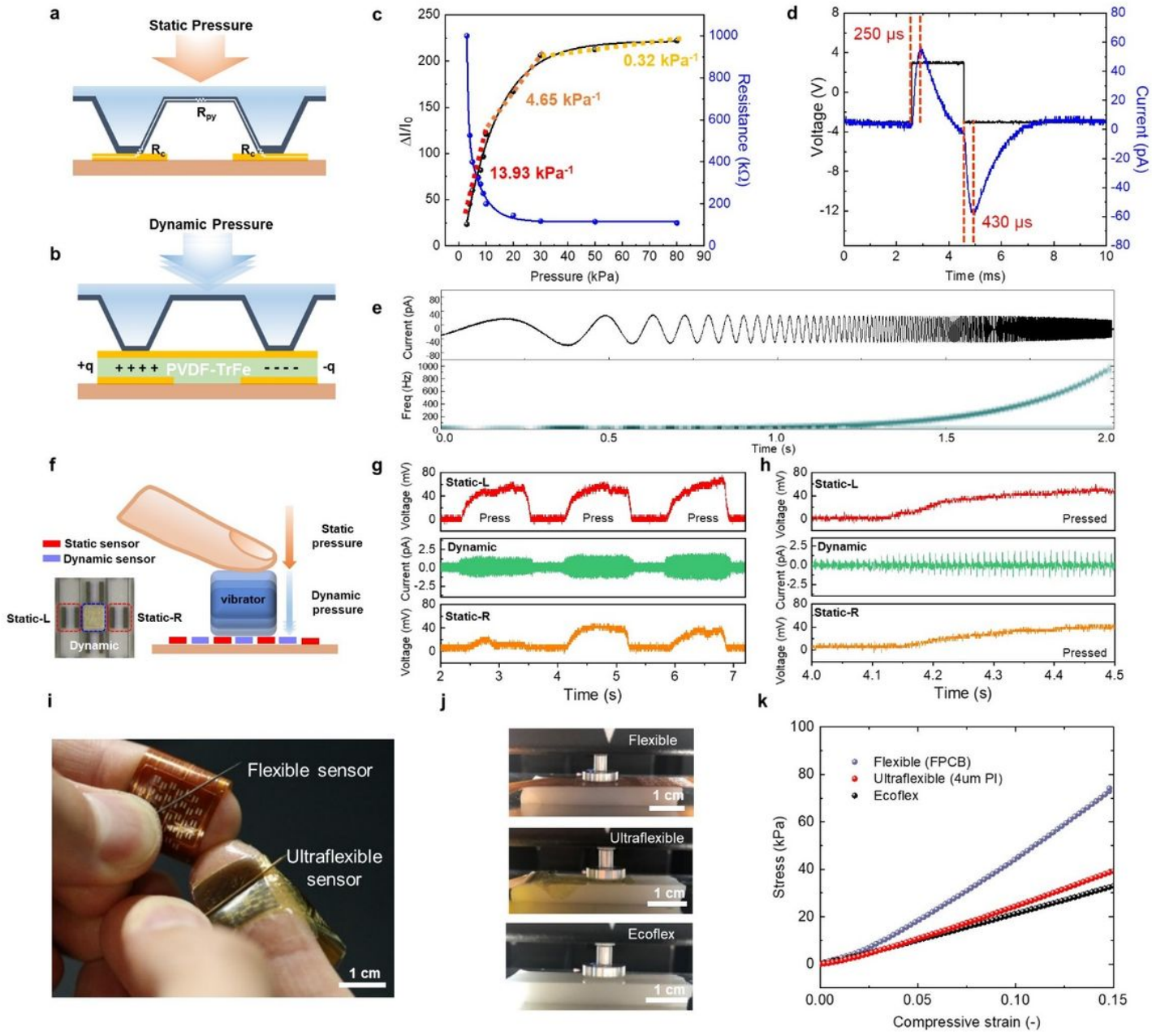

Figure 2

Ultra-flexible bimodal tactile sensor array for tactile acquisition. a, Schematic of piezoresistive static pressure sensor. Polypyrrole coated micro-pyramids make contact with interdigit electrodes under pressure. b, Schematic of piezoelectric dynamic pressure sensor. PVDF-TrFE film generates charges under dynamic pressure. c, Characteristics of piezoresistive static pressure sensor showing the change in current and resistance in the pressure range from 3 to 80 kPa. Pressure sensitivity is plotted with dotted line. d, Response time of piezoelectric dynamic pressure sensor, the black line is the input square wave of the vibrator, the blue line is the output current of the dynamic sensor. e, The frequency response of dynamic pressure sensor from 1 Hz to 1 kHz. Sensor output current (top), STFT spectrogram of sensor output (bottom). f, Schematic of simultaneous monitoring of static and dynamic complex pressure by using UFB tactile sensor array. g, Selective detection of static/dynamic pressure by UFB tactile sensor

array. h, Magnified plot of static and dynamic sensor signals. i, Image of surface deformation while the attached UFB tactile sensor is pressed by a needle. j, Images of the mechanical conformability test setup. k, Strain-stress curve of flexible substrate and ultra-flexible compressive strain. Conventional flexible substrate shows 3 times higher modulus than the UFB sensor.

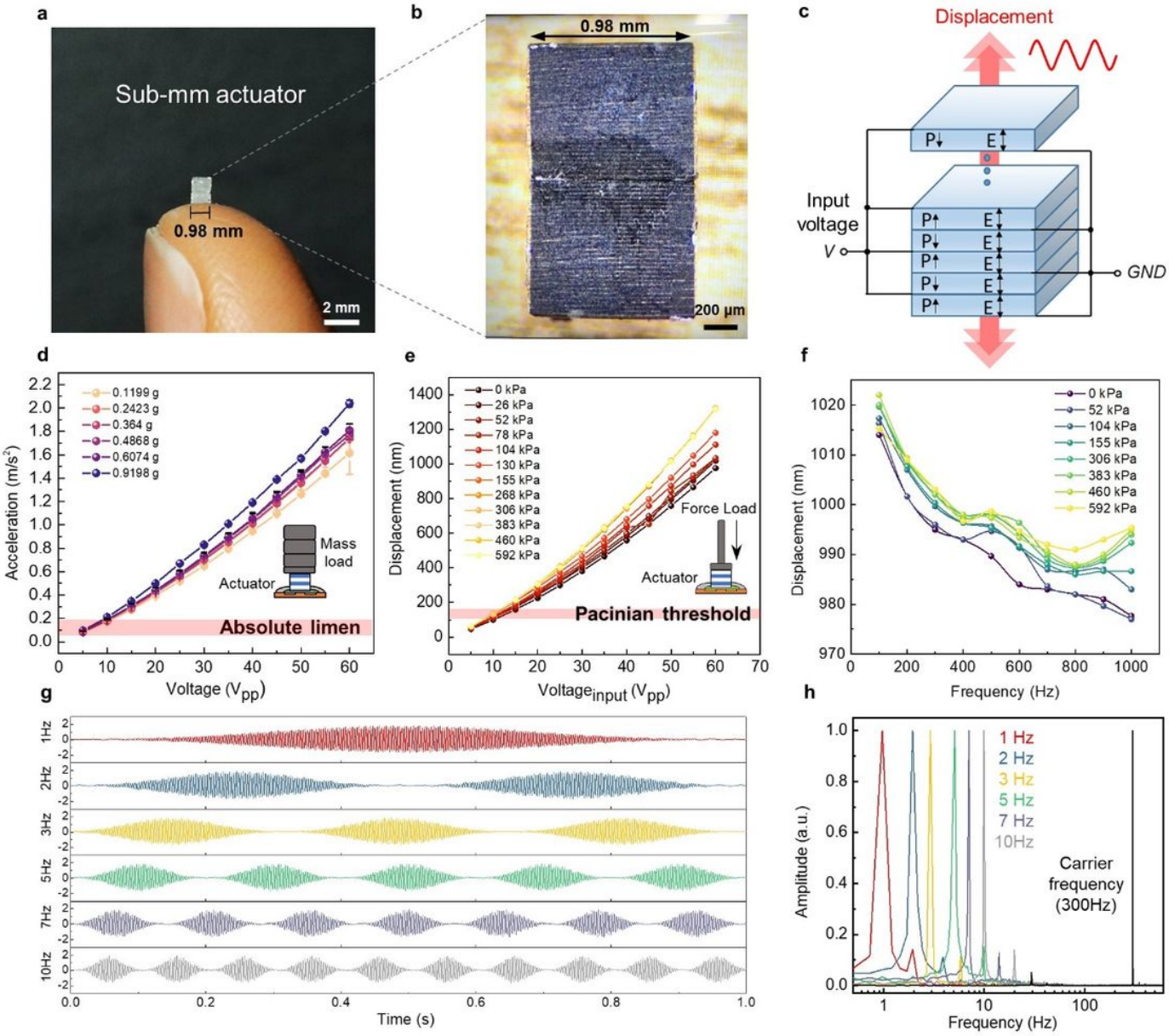

Figure 3

Flexible sub-mm tactile actuator array for tactile rendering. a, Image of a single actuator unit on a fingertip. b, Optical microscope image of sub-mm tactile actuator. Multi-stack piezo ceramic block is miniaturised for high-resolution tactile rendering. c, Schematic of multi-layered piezoelectric actuator. d, Acceleration of a single actuator under various mass loading while input voltage is applied from 5 to 60 Vpp with standard deviation (SD) error bars. e, Displacement of a single actuator under pressure loading while input voltage is applied from 5 to 60 Vpp. f, Frequency dependence of single actuator under

pressure loading. Graph shows output displacement while frequency is changed from 100 Hz to 1000 Hz. g, Amplitude modulation of sub-mm piezo actuator for expression of static pressure feeling. Low frequency of 1–10 Hz has been demonstrated with a carrier frequency of 300 Hz. h, FFT result of amplitude modulation of sub-mm piezo actuator.

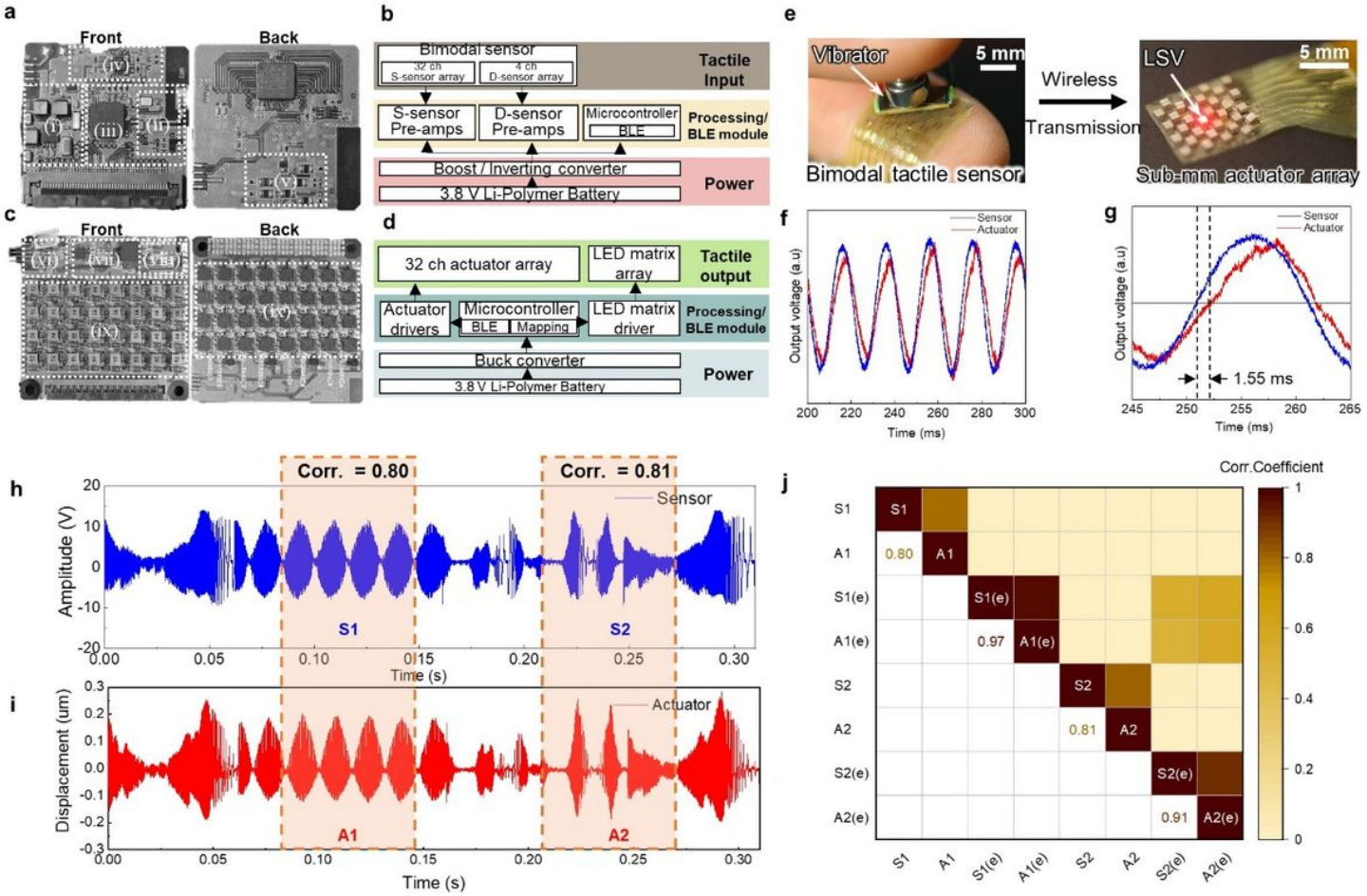

Figure 4

Wireless tactile acquisition and rendering system for telehaptic communication. a, Image of wireless tactile acquisition module. It illustrates the integrated circuit components of the UFB sensor array: (i) boost/inverting converter, (ii) BLE module, (iii) Microcontroller, (iv) 4 ch D-sensor array, and (v) 32 ch S-sensor array. b, System block diagram of tactile acquisition from the UFB sensor array. c, Image of wireless tactile rendering circuit board: (vi) Buck converter, (vii) Microcontroller, (viii) BLE, and (ix) 32 ch actuator drivers. d, System block diagram of tactile rendering from a flexible sub-mm tactile actuator array. e, Image of the UFB tactile sensor (left) applying tactile stimuli patterns with a vibrator. The sub-mm actuator array (right) measures the vibration amplitude and the acceleration using a laser surface velocimeter. f, Wireless transmission of tactile stimuli. The sensor output voltage (red) and actuator vibration velocity (blue) were measured while tactile stimuli of 50 Hz were applied to the sensor using a vibrator. g, The delay time while the sensor signal was transmitted to the actuator board, and the vibration

of the actuator was measured by LSV. h, The acquired tactile sensor output voltage, while random tactile stimuli patterns were applied by the vibrator. i, Vibrational displacement of the tactile actuator rendered by transmitted sensor signals. j, Correlation matrix correlogram of vibration signal pattern of motorcycle describing the correlation coefficient between the signals acquired by the sensor (S1, S2) and the rendered actuator signals (A1, A2). The S1(e), S2(e) and A1(e), A2(e) were envelope of sensor and actuator signals, respectively.

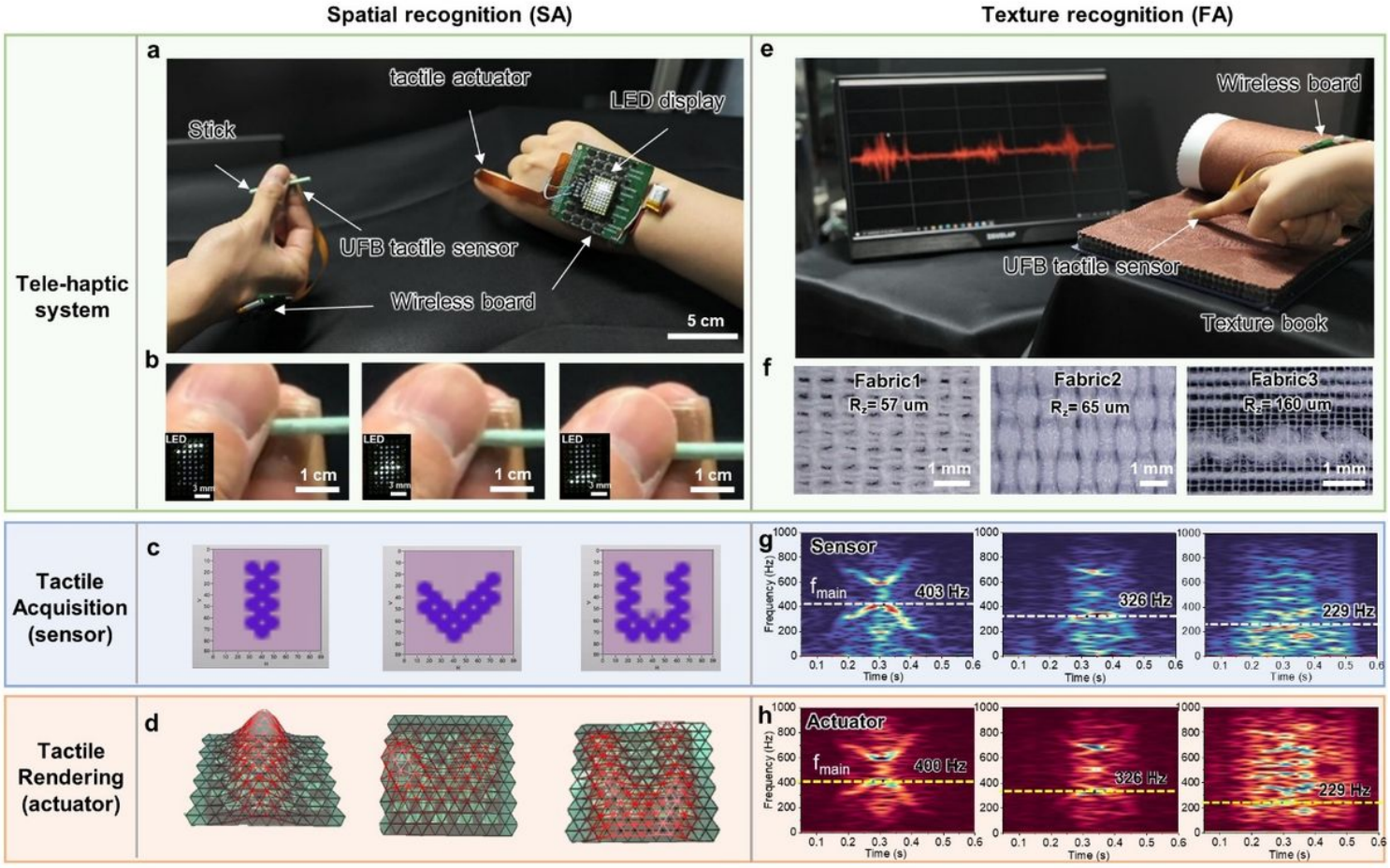

Figure 5

Demonstration of a wireless telehaptic system. a, Spatial information of tactile stimuli (static pressure) was acquired by UFB tactile sensor array and the signals were wirelessly transmitted to the actuator by the telehaptic system. Pressed pixel and pressure scale were visualised by the LED display. b, Magnified image of pressed positions (top, centre, bottom) on the UFB tactile sensor by a stick. Insets are illuminated LED pixels indicating sensor signal for each position. c, Pressure in the form of letter shapes (I, V, U) was applied to the UFB tactile sensor and displayed by the GUI. d, 3D scan image vibrational displacement while acquiring sensor signals rendered by the actuator array. e, Texture information (dynamic pressure) was acquired by UFB sensor while rubbing the different fabrics. f, 3 different types of fabric with various roughness. Fabric 1 is rough, fabric 2 is smooth, and fabric 3 is bumpy because of the height differences in the fibre bundles. g, STFT spectrogram of sensor signal corresponding to fabric 1

(left), fabric 2 (centre), and fabric 3 (right). h, STFT spectrogram of the measured vibration velocity of the actuator for each fabric.

Supplementary Files

This is a list of supplementary files associated with this preprint. Click to download.

- SupplementaryVideos.zip
- SupplementaryInformation.docx